

**Influence of pulsed laser heating on morphological relaxation of surface ripples**

M. Khenner

*Department of Mathematics, State University of New York at Buffalo, Buffalo, New York 14260, USA*

(Received 27 December 2004; revised manuscript received 29 March 2005; published 15 July 2005)

A continuum (Mullins-type) model is proposed for the nonisothermal, isotropic evolution of a crystal surface on which mass transport occurs by surface diffusion. The departure from constant temperature is assumed induced by incident pulsed radiation. It has been shown experimentally and theoretically [see, e.g., Yakunkin, *High Temp.* **26**, 585 (1988); Yilbas and Kalyon, *J. Phys. D.* **34**, 222 (2001)] that such a heating mode gives rise to the quasistationary regime, in which the surface temperature of a thick solid film oscillates about the mean value with the pulse repetition frequency. The implications of oscillatory driving with high frequency values on relaxation of surface ripples are examined; in particular, the traveling wave solutions with decreasing amplitude are detected numerically. Pulsed heating also results in faster smoothing of the ripple, compared to the case when the surface is at constant temperature which is same as the mean temperature in the pulsed heating mode. Impact on ripple shape is minor for ripple amplitudes considered.

DOI: [10.1103/PhysRevE.72.011604](https://doi.org/10.1103/PhysRevE.72.011604)

PACS number(s): 81.10.-h, 68.35.Fx, 68.55.Jk

**I. INTRODUCTION**

Diffusion of adsorbed atoms (adatoms) on surfaces of crystalline thin films is the primary mass transport mechanism responsible for morphological evolution. Surface diffusion coupled to an impinging flux of particles (crystal growth) [1–3] or lattice mismatch stress [4,5] often result in the formation of patterns such as, for example, the pyramidal structures [6,7].

Recently, experimental efforts have been undertaken on assessing effects of pulsed laser beams on surface diffusion of adatoms and molecules [8–10]. These studies characterize the motion of individual particles across the surface using scanning tunneling microscopy and focus primarily on the role of electronic excitation in diffusion. The electronically excited motion is often accompanied by thermally excited motion; the separation of two effects is often difficult.

In a separate line of research, oscillatory driving of surface diffusion has been proposed [11] as an alternative route for pattern formation, “with two basic advantages: First, patterning and growth are separated, so that morphology is not a function of the growth process. Second, it offers better control of the structure. An *in situ* and real-time control of the pattern becomes possible, opening a wide range of new applications.” In Ref. [11] a pulsed laser has been suggested as potentially capable of inducing the oscillatory driving. Work [11] employs a mesoscopic step-flow model for the crystal surface. The adatom diffusivity, kinetic attachment coefficients, and equilibrium concentration are assumed periodically oscillating in time about the respective mean values. Slope selection, surface metastability, and driving frequency-dependent surface stability have been found. Thus oscillatory driving of crystal surfaces has the potential to demonstrate rich nonlinear phenomena similar to one found in other branches of physics; the inverted pendulum problem and pattern formation in oscillatory driven fluids and granular media are two of the many examples (see references in Ref. [11]).

This paper theoretically studies (using the macroscopic, continuum framework) the implications of oscillatory changes of surface temperature on morphological evolution

of a crystal surface by surface diffusion. It is assumed that surface temperature modulation is caused by a low-energy, pulsed laser beam [12]. The classical problem of smoothing of a surface ripple [13] has been chosen for a study.

The paper proceeds as follows. The mathematical model is formulated in Sec. II. In Sec. II A the model form for the temperature perturbation at the surface is discussed, and the equation averaging procedure is employed. Section II B introduces physical parameters, nondimensionalization, and the numerical method. Results are presented in Sec. III, and conclusions in Sec. IV.

**II. MATHEMATICAL MODEL**

Considered is a model 1+1 case corresponding to a two-dimensional crystal with a one-dimensional surface. The evolution of the crystal surface  $z=h(x,t)$  is described by the following phenomenological partial differential equation [13–15]:

$$\frac{h_t}{(1+h_x^2)^{1/2}} = V = -\Omega \cdot js, \quad (1)$$

where  $V$  is the normal velocity of the curve representing the surface,  $\Omega = \text{const}$  the atomic volume,  $j$  the surface diffusion flux, and  $s$  the arclength along the curve. Subscripts denote differentiation in all equations in the paper.

The surface mass flux  $j$  is given by

$$j = -\frac{D(T)\nu}{kT} \mu_s, \quad (2)$$

where  $\nu = \text{const}$  is the surface density of adatoms,  $k$  the Boltzmann constant,  $T$  the temperature,

$$D(T) = D_0 \exp\left(\frac{-E_d}{kT}\right) \quad (3)$$

the surface diffusivity of adatoms, and

$$\mu = \Omega \gamma \kappa \quad (4)$$

the surface chemical potential. In Eq. (3),  $D_0 = \text{const}$  and  $E_d = \text{const}$  are the prefactor and activation energy, respectively. In Eq. (4),  $\gamma$  is the isotropic surface energy density and

$$\kappa = \frac{-h_{xx}}{(1+h_x^2)^{3/2}} \quad (5)$$

the surface mean curvature. Equation (2) holds for the regime where the kinetics of mass transport is determined by diffusion on terraces.

Substitution of Eqs. (2)–(5) into Eq. (1) and using  $\partial/\partial s = (1+h_x^2)^{-1/2} \partial/\partial x$  yields the following fourth-order surface evolution equation:

$$h_t = B \frac{\partial}{\partial x} \left( \frac{\exp(-E_d/kT)}{kT} (1+h_x^2)^{-1/2} \left[ \frac{-h_{xx}}{(1+h_x^2)^{3/2}} \right]_x \right), \quad (6)$$

where  $B = \Omega^2 \nu D_0 \gamma$

The horizontal dimension of the spatially modulated (rippled) surface is  $L$ .  $\ell$  is a constant integer number of ripple wavelengths per  $L$ . Then  $\lambda = L/\ell$  is the wavelength of the ripple and  $q = 2\pi/\lambda$  is the wave number. Assume the entire surface is irradiated by laser pulses.

Equation (6) admits trivial solution (equilibrium state)

$$h = h_0 = \text{const} \quad (7)$$

at any temperature  $T = T(x, t)$ . Without loss of generality  $h_0 = 0$  can be chosen. When pulsed laser heating is applied to the surface for a sufficiently long period of time, a quasistationary regime develops, which is characterized by the mean temperature  $T_0 = \text{const} > T_a$  (where  $T_a$  is ambient temperature; for instance,  $T_a$  could be the temperature of vacuum furnace) and small temperature oscillations on this background [16,17]. Consider perturbation of the equilibrium state  $h = \tilde{h}(x, t)$ , and simultaneous perturbation of the mean temperature field,  $T = T_0 + \tilde{T}(x, t)$ , such that

$$\left| \frac{\tilde{T}(x, t)}{T_0} \right| \equiv |\hat{T}(x, t)| \ll 1, \quad \tilde{h}(x, 0) = H_0 \cos qx, \quad (8)$$

and  $|\tilde{h}(x, t)|$  is not necessarily small.

Next, the quotient  $\exp(-E_d/kT_0(1+\hat{T}))/\{kT_0(1+\hat{T})\}$  in Eq. (6) is expanded in powers of small quantity  $\hat{T}(x, t)$ , and the expression in parenthesis is differentiated with respect to  $x$ . This yields

$$h_t = BP_{n-1}(\hat{T}) \hat{T}_x (1+h_x^2)^{-1/2} \left[ \frac{-h_{xx}}{(1+h_x^2)^{3/2}} \right]_x + BP_n(\hat{T}) \times \left\{ (1+h_x^2)^{-1/2} \left[ \frac{-h_{xx}}{(1+h_x^2)^{3/2}} \right]_x \right\}, \quad (9)$$

where  $P_n(\hat{T})$  and  $P_{n-1}(\hat{T}) = dP_n/d\hat{T}$  are polynomials of degrees  $n$  and  $n-1$ , respectively. The tilde sign over  $\tilde{h}(x, t)$  has been omitted. Cases  $n=2, 4, 6$  will be examined; such choice is explained in the next section. The coefficients of the poly-

nomials  $P_n$  and  $P_{n-1}$  are  $\{a_j\}$  and  $\{ja_j\}$ ,  $j=0, \dots, n$ , respectively, viz.

$$a_6 = a_0 \left( \frac{g_0^6}{720} - \frac{g_0^5}{20} + \frac{5}{8} g_0^4 - \frac{10}{3} g_0^3 + \frac{15}{2} g_0^2 - 6g_0 + 1 \right), \quad (10)$$

$$a_5 = a_0 \left( \frac{g_0^5}{120} - \frac{5}{24} g_0^4 + \frac{5}{3} g_0^3 - 5g_0^2 + 5g_0 + 24 \right), \quad (11)$$

$$a_4 = a_0 \left( \frac{g_0^4}{24} - \frac{5}{6} g_0^3 + 3g_0^2 - 4g_0 + 1 \right),$$

$$a_3 = a_0 \left( \frac{g_0^3}{6} - \frac{3}{2} g_0^2 + 3g_0 - 1 \right), \quad (12)$$

$$a_2 = a_0 \left( \frac{g_0^2}{2} - 2g_0 + 1 \right), \quad a_1 = a_0(g_0 - 1) \quad (13)$$

and

$$a_0 = \frac{\exp(-g_0)}{kT_0}, \quad (14)$$

where

$$g_0 = \frac{E_d}{kT_0}. \quad (15)$$

The coefficients have dimension of inverse energy.

Equation (9) is general in the sense that it admits any small perturbation of the mean surface temperature field  $T_0$ . The particular choice for the perturbation is discussed in the next section.

### A. Model for the temperature perturbation

Pulsed irradiation of a crystal surface gives rise to a quasistationary state in which temperature at the targeted spot fluctuates about the mean value  $T_0$  with a frequency equal to the source pulse repetition frequency  $\omega$ . With the goal of modeling the effects produced by pulsed irradiation the simplest model form for the perturbation  $\hat{T}(x, t)$  is postulated:

$$\hat{T}(x, t) = (\cos \omega t) [Q_0 + Q_1 h_* \cos(qx + \beta)], \quad (16)$$

where  $0 < Q_0, Q_1 h_* \ll 1$ ,  $h_*$  is nondimensionalized  $h$  (see Sec. II B for units), and  $\beta$  is the phase shift of the modulation with respect to the ripple. The values of  $T_0, Q_0$ , and  $Q_1$  are determined by the impulsive power density and the mean power density of the radiation, the absorptivity of the surface at the radiation wavelength, and the thermophysical and optical characteristics of the material [16–19].

The periodicity in time of the perturbation is the consequence of the well-developed quasistationary regime, as the result of the pulsed irradiation. The two terms in Eq. (16) model the quasistationary regime on the rippled, evolving surface of a solid film. Note that as  $h_* \rightarrow 0$  only the first term remains, which describes the quasistationary regime on a

flat, horizontal, and stationary surface. The proportionality of the amplitude of the second term to first power of  $h_*$ , and the spatially periodic form are assumed after Refs. [18,19], where the related theories of formation of laser-induced surface ripples (LISRs) were developed; see also the review paper [20].

Works [18,19] and others justify the spatially periodic surface temperature as follows. First, it is assumed that an initial sinusoidal temperature disturbance of period  $\lambda$  exists on the initial surface. This disturbance “may be caused by the height variation itself, by the poor crystalline quality of the surface layer, or by any other intrinsic or extrinsic cause. ... Since the index of refraction of such a surface is temperature dependent, it will also follow a similar periodic variation. The index variation then acts like a ripple, and the light intensity, and therefore the power absorbed, also becomes modulated *with the same period*. The phase of this modulation, however, may or may not reinforce the initial temperature disturbance” [19]. Models of LISRs based on the assumption of the spatially periodic surface temperature during irradiation of the rippled surface match experimental observations reasonably well [20]. The experimental validation of this assumption has been provided in [21]. The key difference between LISRs and the subject under consideration in this work must be emphasized here: LISRs are due to surface melting and recrystallization under the influence of high-energy irradiation, which are not allowed for surface-diffusion driven morphological evolution of the surface shape. It must be noted also that the laser beam-surface interaction mode resulting in the spatially periodic surface temperature field (namely, the interference between incident and scattered light waves) is not universal; quite often there is no such interference and in such cases the second term in Eq. (16) cannot be justified [22]. The case of a spatially uniform temperature field ( $Q_1=0$ ) is considered in Sec. III B. This case provides the most transparent illustration of the smoothing aspect of the pulsed heating effect.

It must be noted that the simple form of the time-dependent amplitude in Eq. (16) is the idealization required in order to obtain a tractable and computationally robust model. The oscillograms of the amplitude of temperature perturbation on the flat specimen surface presented in Ref. [16] are not exactly sinusoidal, and neither are the oscillograms of the output laser pulse; in fact, the output from the laser is not easily fitted by a simple mathematical expression. Also, at  $z=0$  the analytical solution of the one-dimensional (along negative segment of the  $z$  axis) heat conduction problem calculated in Ref. [16] is infinite Fourier series, whose terms have amplitudes decaying as  $j^{-2}$  ( $j=1, \dots, \infty$  is the term number). It is natural to expect that the difference between the model amplitude and the amplitude calculated in Ref. [16] may only be responsible for a small quantitative difference in results. A somewhat more complicated analytical solution of a similar heat conduction problem under conditions of pulsed laser heating of a surface was obtained in Ref. [17]. There, “in order to obtain a *constant* temperature heating condition at the surface, repetitive laser pulses with constructively decaying peak intensities are considered.” The temporal variation of the surface temperature is periodic with the shape close to sinusoidal when this constraint is relaxed.

Both solutions assume a flat surface of the specimen (roughness is not taken into account). However, the quasistationary state does not cease to exist on the rough surface. In other words, for “large” times the one-dimensional heat conduction equation has oscillatory solutions when the boundary condition is imposed on the surface  $z=h(x) \neq 0$ , or even on  $z=h(x,t)$ , rather than on  $z=0$ ; for the latter case to hold, the characteristic time of the development of the quasistationary regime must be much less than the characteristic time of surface morphological evolution. Assume it is indeed so [23].

The problem (9)–(16) has two time scales. These scales are the period of pulse repetition  $t_p=1/\omega$ , and the characteristic time of ripple relaxation at constant  $T=T_0$ . This latter scale is the time it takes the surface diffusion to diminish the initial amplitude of the ripple by  $e$  times, and it is given by  $t_s=(Ba_0q^4)^{-1}$ . The case of high pulse repetition frequency will be considered, so that  $t_p \ll t_s$ . In this limit the ripple relaxation on the long time scale  $t_s$  can be studied using Eq. (9) where the time- and space-periodic functions  $BP_{n-1}(\hat{T})\hat{T}_x$  and  $BP_n(\hat{T})$  are averaged over the temporal period of oscillation. The averaging procedure reduces to zero such terms in the latter function that correspond to odd powers of  $\hat{T}(x,t)$ , and also such terms in the former function that correspond to an odd sum of powers of  $\hat{T}(x,t)$  and  $\hat{T}_x(x,t)$ . That explains the choice of even polynomial degree for these functions. The averaged evolution Eq. (9) reads

$$h_t = -BU(x,t)(1+h_x^2)^{-1/2} \left[ \frac{-h_{xx}}{(1+h_x^2)^{3/2}} \right]_x + BV(x,t) \left\{ (1+h_x^2)^{-1/2} \left[ \frac{-h_{xx}}{(1+h_x^2)^{3/2}} \right]_x \right\}, \quad (17)$$

where

$$U(x,t) = \begin{cases} a_2\sigma_x\sigma \equiv u_2(x,t) & \text{if } n=2, \\ u_2(x,t) + (3/2)a_4\sigma_x\sigma^3 \equiv u_4(x,t) & \text{if } n=4, \\ u_4(x,t) + (15/8)a_6\sigma_x\sigma^5 & \text{if } n=6, \end{cases} \quad (18)$$

$$V(x,t) = \begin{cases} a_0 + (1/2)a_2\sigma^2 \equiv v_2(x,t) & \text{if } n=2, \\ v_2(x,t) + (3/8)a_4\sigma^4 \equiv v_4(x,t) & \text{if } n=4, \\ v_4(x,t) + (5/16)a_6\sigma^6 & \text{if } n=6, \end{cases} \quad (19)$$

and

$$\sigma(x,t) = Q_0 + Q_1h_* \cos(qx + \beta). \quad (20)$$

A frequently used framework for studying surface evolution problems is the small-slope approximation, which is applicable when the surface slope  $|h_x| \ll 1$  for all times. If this is the case, the governing PDE can be expanded in powers of the small quantity  $h_x$ . This procedure, especially when it is followed by linearization, often leads to simplification of the equation. Then, the solution could be attempted analytically. For the problem under consideration in this paper, the small-

slope approximation is of no particular advantage since it generally does not yield the analytically tractable problem due to the complicated structure of functions  $U$  and  $V$  in Eq. (17). However, notice that in the case  $n=1$  (which corresponds to the first order of the expansion in the temperature perturbation, such that  $P_0=a_1$  and  $P_1=a_0+a_1\hat{T}$ ) the small-slope, averaged evolution equation describes the isothermal relaxation of the ripple to the equilibrium state  $h_0=0$ , at temperature  $T_0$ :

$$h_t = Ba_0 Y(x, t), \quad (21)$$

where

$$Y(x, t) = -h_{xxxx} + 3h_{xx}^3 + 10h_{xx}h_{xxx}h_x + 2h_{xxxx}h_x^2. \quad (22)$$

Equation (22) is correct to sixth order, since  $\partial/\partial x \sim \epsilon \ll 1$ . In particular, Eq. (21) yields the monotonous exponential decay solution in the linear approximation  $Y(x, t) = -h_{xxxx}$ :

$$h(x, t) = H_0 \exp(-Ba_0 q^4 t) \cos qx, \quad (23)$$

which preserves the initial sinusoidal shape of the ripple (see Eq. (8)). This solution was obtained by Mullins [13]. The nontrivial small-slope, averaged evolution equation results at least in the second order of the expansion in  $\hat{T}(x, t)$ . This corresponds to the second order nontrivial, averaged surface flux in the step-flow model of Ref. [11].

Next, the transparent illustration of the origin of the pulsed heating effect is provided.

Let  $D_*(T) = \exp(-E_d/\{kT\})/\{kT\}$ , refer to Eq. (6). Let  $Q_1=0$  for simplicity. Expanding  $D_*(T)$  in powers of  $\tilde{T}$  about  $T_0$  up to second order, then noticing that  $\tilde{T}=T_0\hat{T}$  and averaging over  $2\pi/\omega$  yields

$$\langle D_*(T) \rangle = D_*(T_0) + \frac{1}{2} D_*''(T_0) \left( \frac{1}{2} T_0^2 Q_0^2 \right), \quad (24)$$

where  $\langle \cdot \rangle$  denotes averaged quantity. Since

$$D_*''(T_0) = \frac{2a_2}{T_0^2}, \quad (25)$$

Eq. (24) becomes

$$\langle D_*(T) \rangle = D_*(T_0) + \frac{1}{2} a_2 Q_0^2. \quad (26)$$

Thus it is expected that the pulsed heating results, primarily, in increased effective diffusivity (since  $a_2$  is positive for the typical material system under consideration, see the next section) and therefore, in faster morphological relaxation.

### B. Choice of parameters

Equation (17) is now nondimensionalized;  $1/\omega$  is used for unit of time and  $L$  for unit of length. The nondimensional equation is (star sign has been omitted)

$$h_t = -\bar{B} \left[ \bar{U}(x, t) (1 + h_x^2)^{-1/2} \left[ \frac{-h_{xx}}{(1 + h_x^2)^{3/2}} \right]_x - \bar{V}(x, t) \left\{ (1 + h_x^2)^{-1/2} \left[ \frac{-h_{xx}}{(1 + h_x^2)^{3/2}} \right]_x \right\}_x \right], \quad (27)$$

where

$$\bar{U}(x, t) = \begin{cases} \bar{\sigma}_x \bar{\sigma} \equiv \bar{u}_2(x, t) & \text{if } n=2, \\ \bar{u}_2(x, t) + (3/2) A_2 \bar{\sigma}_x \bar{\sigma}^3 \equiv \bar{u}_4(x, t) & \text{if } n=4, \\ \bar{u}_4(x, t) + (15/8) A_3 \bar{\sigma}_x \bar{\sigma}^5 & \text{if } n=6, \end{cases} \quad (28)$$

$$\bar{V}(x, t) = \begin{cases} A_1 + (1/2) \bar{\sigma}^2 \equiv \bar{v}_2(x, t) & \text{if } n=2, \\ \bar{v}_2(x, t) + (3/8) A_2 \bar{\sigma}^4 \equiv \bar{v}_4(x, t) & \text{if } n=4, \\ \bar{v}_4(x, t) + (5/16) A_3 \bar{\sigma}^6 & \text{if } n=6, \end{cases} \quad (29)$$

$$\bar{\sigma}(x, t) = Q_0 + Q_1 h \cos(\bar{q}x + \beta), \quad \bar{q} = 2\pi\ell, \quad (30)$$

and  $\bar{B} = a_2 B / (\omega L^4)$ ,  $A_1 = a_0/a_2$ ,  $A_2 = a_4/a_2$ , and  $A_3 = a_6/a_2$ .

GaAs on GaAs diffusion at  $T_0=800$  K is chosen as an example; the characteristic value of the activation energy at this temperature is  $E_d \approx 0.8$  eV [24]. This yields  $g_0 = 11.4317$  from Eq. (15) and, using Eqs. (10)–(14),  $A_1 = 0.023$ ,  $A_2 = -4.28$ , and  $A_3 = -1.27$ . Value  $0.14$  cm<sup>2</sup>/s for the diffusivity prefactor  $D_0$  is obtained using the above cited  $E_d, T_0$  values, and a value of  $1.5 \times 10^{-6}$  cm<sup>2</sup>/s for diffusivity [24]. Also, at typical values  $L = 10$  μm,  $\Omega = 2 \times 10^{-23}$  cm<sup>3</sup>,  $\gamma = 10^3$  erg/cm<sup>2</sup>,  $\nu = 10^{15}$  cm<sup>-2</sup>, and  $\omega = 10^4$  s<sup>-1</sup>, one obtains  $t_p = 10^{-4}$  s,  $t_s = 4.5 \times 10^2$  s, and  $\bar{B} \approx 2.4 \times 10^{-11}$ , given  $\ell = 4$ . Since the value of  $\ell$  determines the wave number of the ripple and thus the characteristic time  $t_s$ , it has been chosen to ensure  $t_s \gg t_p$ . This admissibility criteria allows  $\ell$  as large as  $\sim 50$ .

The method of lines approach was used for computations. Standard second-order finite differencing in space was implemented, and time stepping was done using the implicit Runge-Kutta method [25]. Boundary conditions at  $x=0, 1$  are periodic. By closely examining Eq. (27) it became clear that values  $\beta=0, \pi/2, \pm\pi/4$  are special in the sense that they can either change signs of periodic coefficients, or turn the sine function into the cosine function (or vice versa). Thus only these values were tried in numerical simulation. At  $t=0$  the ripple shape is given by Eq. (8), where the initial amplitude  $H_0$  is replaced by nondimensional initial amplitude  $\bar{H}_0 = H_0/L$ .  $\bar{H}_0$  was taken as 0.02 or 0.08. In all cases the runs were terminated when amplitude at a crest reached the cutoff amplitude  $0.1\bar{H}_0$ . For all numerical experiments spatial resolution is  $\Delta x = 0.002$ , and relative and absolute tolerances of the implicit RK solver are  $10^{-10}$  and  $10^{-8}$ , respectively.

The following nondimensional equation will be used for comparison purposes when  $\bar{H}_0 = 0.02$ :

$$h_t = \Lambda \left\{ (1 + h_x^2)^{-1/2} \left[ \frac{-h_{xx}}{(1 + h_x^2)^{3/2}} \right]_x \right\}, \quad (31)$$

$$\Lambda = \frac{B}{\omega L^4 k T_0 (1 + i Q_0)}, \quad i = 0, \pm 1. \quad (32)$$

Equation (31) describes the *isothermal* surface evolution (that is, when pulsed heating is not applied). The three situations distinguished next all correspond to the surface temperature held elevated over ambient temperature.

- (1)  $i=0$  and  $T=T_0$ . In this case  $\Lambda = \bar{B}A_1 = 5.52 \times 10^{-13}$ .
  - (2)  $i=1$  and  $T=T_0(1+Q_0)$ . The parameters for this case are  $g_1 = 10.3896$  and  $\Lambda = 1.4 \times 10^{-12}$ , given  $Q_0 = 0.1$ . The case corresponds to the almost maximal attainable surface temperature in the pulsed heating regime [since the magnitude of the second term in Eq. (30) is less than or equal to one-tenth of the magnitude of the first term there, for  $Q_0 = 0.1, Q_1 = 0.5$ , and for  $|h| \leq 0.02$ ].
  - (3)  $i=-1$  and  $T=T_0(1-Q_0)$ . This corresponds to the almost minimal attainable surface temperature in the case of pulsed heating. The parameters for this case are  $g_{-1} = 12.6984$  and  $\Lambda = 1.7 \times 10^{-13}$ , given  $Q_0 = 0.1$ .
- $1/\omega$  has been used as a unit of time for nondimensionalization of the original equation only for convenience, e.g., to avoid introducing an additional nondimensional parameter (of course,  $\omega$  does not have a physical meaning in the absence of pulsed heating). Such a choice does not affect the temporal or spatial evolution of the ripple.

### III. RESULTS

#### A. Small amplitude case

Figure 1 shows the nondimensional amplitudes of the ripple at crests computed using  $n=2, 4$ , and  $6$  terms of the expansion in temperature perturbation. Also shown is the amplitude when pulsed heating is off and the temperature is constant  $T_0$  [refer to Eq. (31)]. Figure 1 does not call for the increase in the number of terms of the expansion beyond  $n=2$ , since the  $n=4, 6$  case results are nearly indistinguishable from the  $n=2$  case result. Nevertheless,  $n=6$  will be used throughout the rest of the paper; more than two terms of the expansion may be needed in case of larger ripple amplitudes. The shape of the ripple is the cosine function for all three values of  $n$ , and also in the isothermal case.

Figure 2 compares the amplitude of the ripple in the pulsed heating case to amplitudes in three isothermal cases.

Figure 3 shows the amplitudes for  $\beta=0, \pi/2$ , and  $\pm\pi/4$ . For all four values of  $\beta$  the ripple shape is the cosine function at all times.

From Figs. 1–3 it can be seen that for any value of the phase shift the ripple under the oscillatory driving about mean temperature  $T_0$  relaxes faster than the ripple held at constant temperature  $T_0$ . Figure 3 shows that for  $Q_0 = 0.1, Q_1 = 5.0$  the relaxation is fastest in the case  $\beta=0$ . In the case  $Q_0 = 0.1, Q_1 = 0.5$  the rates corresponding to all four values of  $\beta$  are almost same, and Fig. 2 shows this curve for  $\beta=0$ .

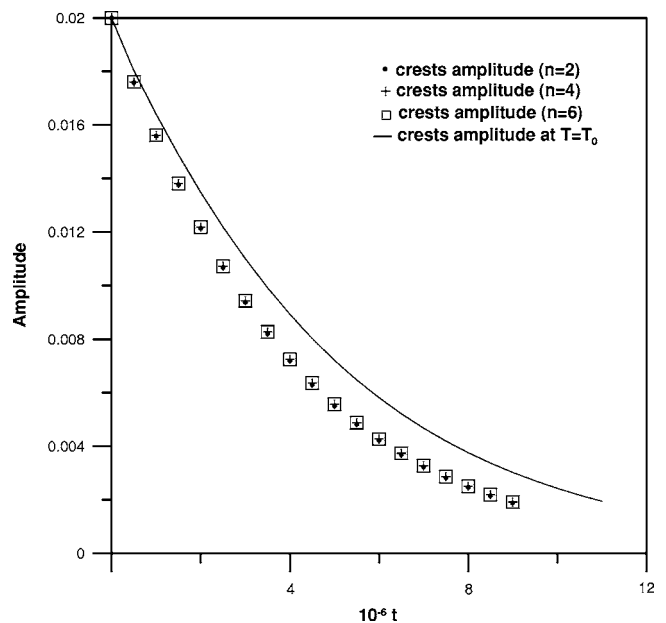


FIG. 1. Test case (convergence study). Comparison of ripple amplitudes using Eq. (27) with  $n=2, 4, 6$ . Solid curve: pulsed heating is off and surface is at constant temperature  $T_0$ .  $Q_0=0.1, Q_1=0.5, \beta=0$ .

#### 1. Traveling waves

In the numerical simulations with  $\beta = \pi/2, \pm\pi/4$  and sufficiently large (but consistent with the formulation) values of  $Q_0$  and  $Q_1$  the ripple undergoes the uniform translation to the left or right with small but detectable speed. In other words, the traveling wave with the decaying amplitude appears on the surface. The direction of the traveling wave depends on magnitudes of  $Q_0$  and  $Q_1$ , as well as on the value of  $\beta$ . For

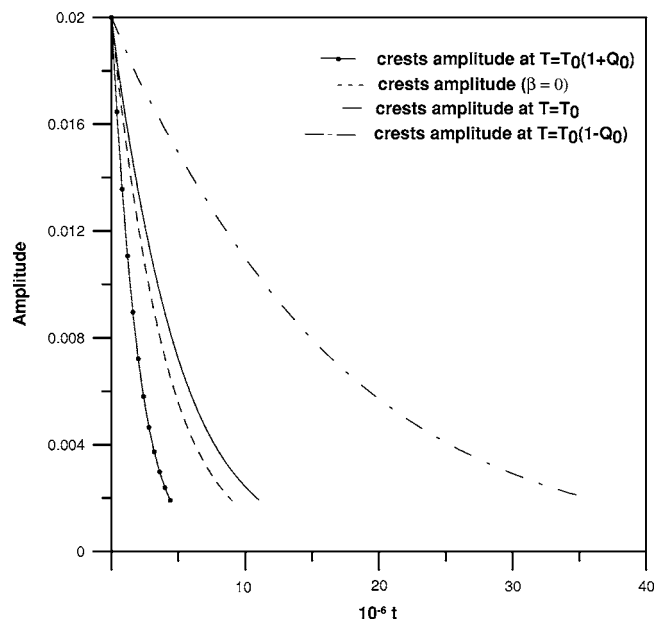


FIG. 2. Comparison of ripple amplitudes for different heating modes (see key). All curves but the dashed one are computed using the “isothermal” Eq. (31).  $Q_0=0.1, Q_1=0.5, \beta=0$ .

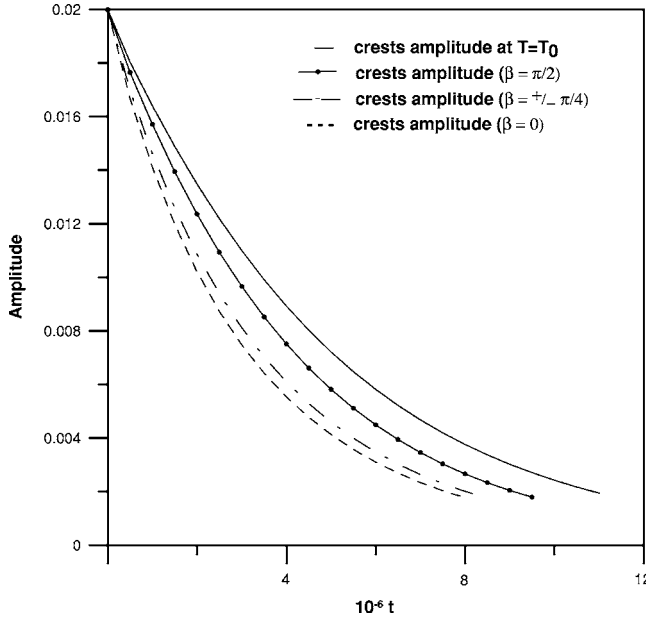


FIG. 3. Amplitude of the ripple given phase shift in Eq. (16) either  $\beta=0$ , or  $\beta=\pm\pi/4$ , or  $\beta=\pi/2$ . Solid curve: pulsed heating is off and surface is at constant temperature  $T_0$ .  $Q_0=0.1, Q_1=5.0$ .

instance, for  $\beta=\pi/2, Q_0=0.1$  and  $Q_1=2.5, 5.0$  the traveling wave direction is to the right, but the direction is opposite for  $Q_0=0.5$  and  $Q_1=2.5$ . Waves always travel in the opposite directions for  $\beta=\pi/4$  and  $-\pi/4$ . For  $\beta=0$  the traveling wave is absent for any values of  $Q_0$  and  $Q_1$ . Recall that  $\beta$  measures the horizontal shift of the temperature perturbation with respect to the ripple. Thus from Fig. 3 the relaxation is the fastest when extrema of the spatially periodic multiplier in Eq. (16) occur at ripple extrema ( $\beta=0$ ), as expected.

As an example, consider case  $\beta=\pi/2$  and  $Q_0=0.1, Q_1=5.0$ . The absolute value of the nondimensional horizontal displacement of the ripple vs nondimensional time is fitted well by quadratic function  $d(t)=1.832 \times 10^{-9}t - 1.029 \times 10^{-16}t^2$ . Thus the speed of the traveling wave is approximately linear,

$$V_{\text{wave}}(t) \approx 1.832 \times 10^{-9} - 2.058 \times 10^{-16}t. \quad (33)$$

The actual displacement has been measured by noticing the amount of a shift from the line  $x=1(x=0)$  that the rightmost (leftmost) point on the ripple incurs when the ripple undergoes translation to left (right).

At least in the special case described below, some insight into the traveling wave solution can be obtained semianalytically. Let  $n=4$  and formally assume the long-wave approximation, for which

$$\begin{aligned} h &= \epsilon h_1 + \epsilon^2 h_2 + \dots, \\ \frac{\partial}{\partial x} &= \epsilon \frac{\partial}{\partial x_1} + \epsilon^2 \frac{\partial}{\partial x_2} + \dots, \quad \frac{\partial}{\partial t} = \epsilon^4 \frac{\partial}{\partial t_4} + \epsilon^5 \frac{\partial}{\partial t_5} + \dots, \\ \epsilon &\ll 1. \end{aligned} \quad (34)$$

Then in the lowest fifth order in  $\epsilon$  Eq. (27) reduces to

$$\begin{aligned} h_t &= -\bar{B}\bar{q}Q_0Q_1 \left( 1 + \frac{3}{2}A_2Q_0^2 \right) \sin(\bar{q}x + \beta) h h_{xxx} - \bar{B} \left( A_1 + \frac{1}{2}Q_0^2 \right. \\ &\quad \left. + \frac{3}{8}A_2Q_0^4 \right) h_{xxxx}, \end{aligned} \quad (35)$$

where the expansion indices have been omitted. Now, the solution of Eq. (35) is sought in the form

$$h = p(t) \cos \bar{q}\xi, \quad \xi = x + w(t)t. \quad (36)$$

Substitution of Eq. (36) in Eq. (35) yields

$$\begin{aligned} (p - Mp) \cos \bar{q}\xi - p \{ \bar{q}(wt + w) + Np \sin[\bar{q}(\xi - wt) \\ + \beta] \cos \bar{q}\xi \} \sin \bar{q}\xi = 0, \end{aligned} \quad (37)$$

where

$$M = -\bar{B}\bar{q}^4 \left( A_1 + \frac{1}{2}Q_0^2 + \frac{3}{8}A_2Q_0^4 \right), \quad (38)$$

$$N = -\bar{B}\bar{q}^4 Q_0 Q_1 \left( 1 + \frac{3}{2}A_2Q_0^2 \right). \quad (39)$$

Since  $\cos \bar{q}\xi$  and  $\sin \bar{q}\xi$  are linearly independent,

$$\dot{p} - Mp = 0, \quad (40)$$

$$\bar{q}(wt + w) + Np \sin[\bar{q}(\xi - wt) + \beta] \cos \bar{q}\xi = 0. \quad (41)$$

The solution of Eq. (40) with initial condition  $p(0)=\bar{H}_0$  is

$$p(t) = \bar{H}_0 \exp(Mt), \quad (42)$$

and thus Eq. (41) yields the following ODE for wave velocity  $w(t)$ :

$$\dot{w} = -\frac{1}{t} \left\{ w + \frac{N}{\bar{q}} \bar{H}_0 \exp(Mt) \sin(\bar{q}x + \beta) \cos[\bar{q}(x + wt)] \right\}, \quad (43)$$

where variable  $x$  has been restored.  $M=-2.6658 \times 10^{-7}$  and  $N=4.4805 \times 10^{-6}$  for parameter values of II B and consider  $x$  fixed in Eq. (43). The first term suggests that  $w$  behaves as  $t^{-1}$ , but it is the second term that in fact determines the characteristic time scale of the decay of a speed of ripple lateral motion. Equation (43) was integrated numerically from  $t=10^{-12}$  to  $t=10^7$  with zero initial condition and some values of  $x$  in  $[0, 1]$ .

$w=0$  to machine precision for  $\beta=0$  and the ripple extreme/zero points.  $w \neq 0$  for other points in  $[0, 1]$ . Thus in the case  $\beta=0$  Eq. (36) implies relaxation in the absence of a traveling wave.

$w < 0 (> 0)$  for  $\beta=\pi/2, \pi/4(-\pi/4)$  and the ripple extreme points; that is, the ripple extrema move to the right (left). The speed of the extreme points is (i) smaller for  $\beta=\pm\pi/4$ , compared to the  $\beta=\pi/2$  case and (ii) same for  $\beta=\pi/4$  or  $-\pi/4$ . For fixed  $\beta$  and different extreme points the function  $w(t)$  is the same. All of the above matches completely the full simulation of ripple relaxation. However,  $w=0$  for ripple zero points and any of the three  $\beta$  values. Thus unlike the simulation of ripple relaxation, the solution obtained in the long

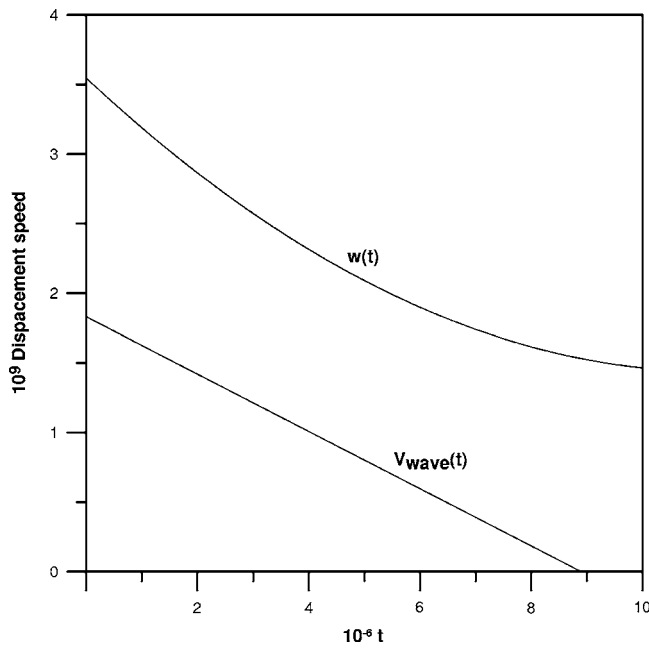


FIG. 4. Speed of ripple displacement. Functions  $V_{\text{wave}}(t)$  and  $w(t)$  are defined in the text.  $\beta = \pi/2, Q_0 = 0.1, Q_1 = 5.0$ .

wave approximation is not a traveling wave, but a lateral ripple deformation that leaves ripple zero points at rest (self-steepening). Nevertheless, Fig. 4 shows the speed  $w(t)$  at ripple extrema, together with the traveling wave speed, Eq. (33), and Fig. 5 shows the amplitude  $p(t)$  together with the relaxation amplitude from the full simulation.

**B. Large amplitude case**

The main difference from the small amplitude case is the shape of the ripple; it slightly deviates from the cosine func-

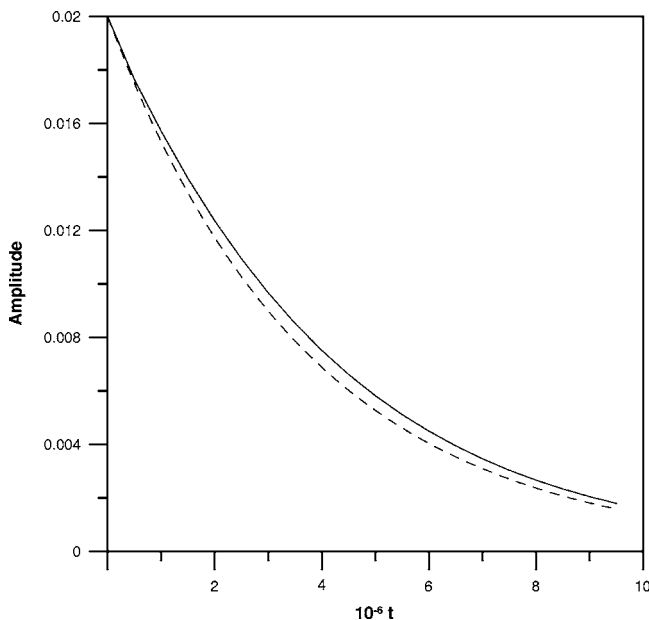


FIG. 5. Amplitude of the ripple. Solid curve: traveling wave amplitude from full simulation. Dashed curve: Eq. (42).  $\beta = \pi/2, Q_0 = 0.1, Q_1 = 5.0$ .

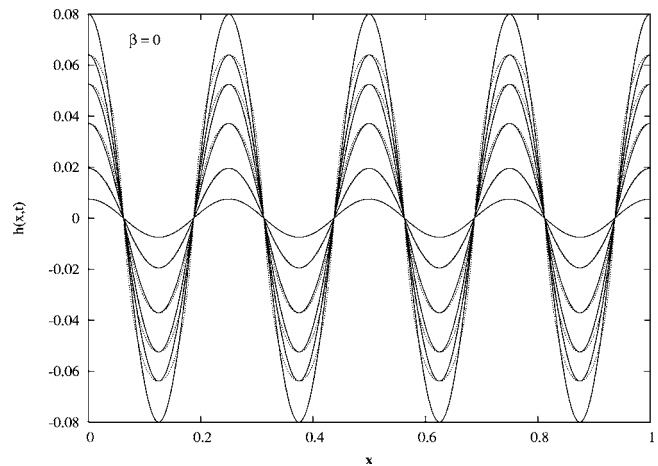


FIG. 6. Ripple smoothing for large initial amplitude and pulsed heating. Dotted curves: the ripple. Solid curves: the cosine function.  $Q_0 = 0.1, Q_1 = 0.5$ .

tion for amplitudes in the range 0.08–0.03 due to, primarily, strong nonlinearity. The contribution of the pulsed heating effect itself in shape deviation is present, but is very small for  $\bar{H}_0 = 0.08$  (that is, almost the same deviation occurs when the pulsed heating is off and the surface is held at constant temperature  $T_0$ ). For smaller amplitudes the ripple shape is indistinguishable from the cosine function, as discussed above. Figure 6 shows both shapes as  $t$  increases. For initial amplitudes larger than 0.08 to 0.09 the computation is generally unsuccessful due to strong numerical stiffness.

**1. Rate of relaxation: Study with varying  $Q_0, Q_1$**

Figure 7 compares relaxation amplitudes resulting from the temperature perturbation with amplitude  $Q_0 = 0.1, 0.075,$

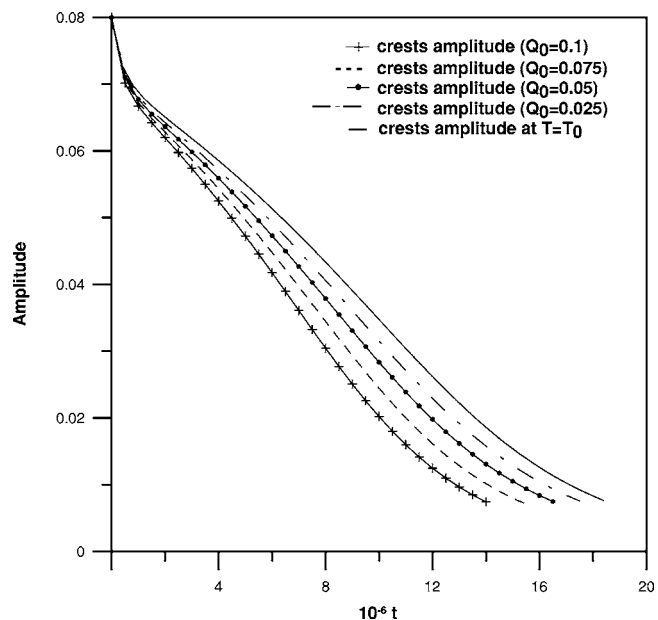


FIG. 7. Comparison of amplitudes for pulsed heating cases with decreasing values of  $Q_0$ .  $\beta = 0, Q_1 = 0.5$ . Solid curve: pulsed heating is off and surface is at constant temperature  $T_0$ .

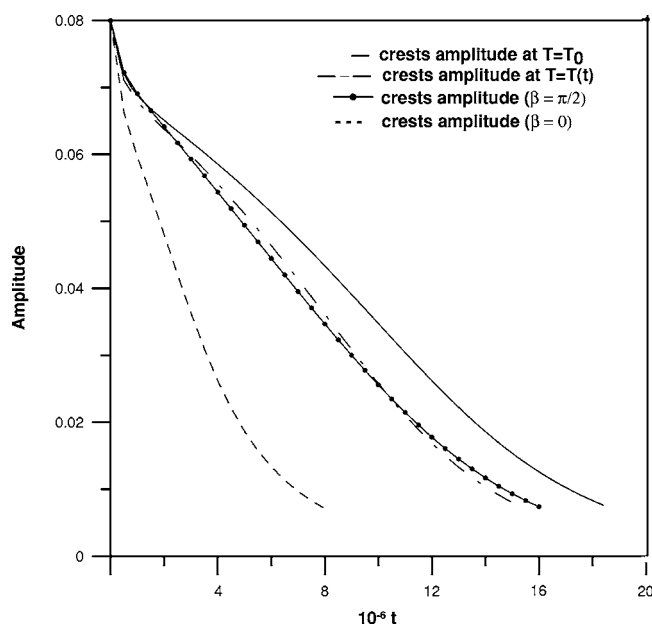


FIG. 8. Comparison of amplitudes for pulsed heating cases  $\hat{T} = \hat{T}(x, t)$  [Eq. (16) with  $Q_0=0.1, Q_1=5.0$ , and  $\beta=0, \pi/2$ ], and  $\hat{T} = \hat{T}(t) = Q_0 \cos \omega t, Q_0=0.1$ . Solid curve: pulsed heating is off and surface is at constant temperature  $T_0$ .

0.05, and 0.025 and fixed amplitude  $Q_1=0.5$ . As  $Q_0 \rightarrow 0$ , the rate of relaxation of the oscillatory driven ripple approaches the rate of relaxation of the isothermal ripple at  $T=T_0$ .

Finally, case  $Q_1=0$  in Eq. (16) is investigated. This case corresponds to time-periodic and spatially uniform temperature perturbation. It can be seen that  $U(x, t)=0$  and  $V(x, t)=\text{const}$  in Eq. (17), and therefore the evolution equation has the same form as in the isothermal case. As discussed in II A, the effect of such temperature perturbation is simply the increase of value of the characteristic (positive) decay constant from its value at constant temperature  $T_0$ . Amplitudes of the ripple, which result when the ripple is smoothed by applying pulsed heating where  $\hat{T}$  is given by Eq. (16), and by reduced Eq. (16) where  $Q_1=0$  are shown in Fig. 8. It can be seen that the ripple relaxes faster when the temperature perturbation is spatially periodic with  $\beta=0$ . Pulsed heating where  $\hat{T}$  is spatially periodic with  $\beta=\pi/2$  is almost as effective as the spatially uniform mode. This is expected since for  $\beta=\pi/2$  the extrema of the spatially periodic multiplier in Eq. (16) occur almost at ripple zero points (since the ripple undergoes a

slow translation to the right) and thus the effect on the rate of relaxation is small.

#### IV. CONCLUSIONS

In summary, this paper suggests a simple, nonlinear continuum model of the driven evolution by nonisothermal surface diffusion (where the temperature oscillations about mean value  $T_0$  are induced by a pulsed laser beam) of the preexisted surface morphology. The numerical simulations demonstrate that rates of smoothing are faster than the classical rate for the isothermal, no oscillations case  $T=T_0$ . Also, the unexpected traveling wave mode of relaxation is detected for some values of the parameter governing the horizontal shift of the (time-oscillatory) temperature perturbation with respect to the ripple.

The promising extensions of this study are:

(i) the inclusion of anisotropic (and temperature-dependent) surface energy density, which has been shown to play a crucial role in the formation of surface structures [3];

(ii) the inclusion of deposition of material on the surface.

Of special interest is interplay of pulsed (oscillatory) deposition and oscillatory driving through the pulsed heating. The two mechanisms acting simultaneously may create *instabilities*. It has been pointed out in [11] that such instabilities may be new and not observed before. This situation reminds the two-frequency driving of a fluid surface [26];

(iii) the inclusion of additional spatial dimension, with or without anisotropy and temperature dependence of the surface tension, and deposition. In particular, the attachment-detachment limited kinetics [27] in 2+1 dimension has been shown to give rise to unusual surface relaxation dynamics [28]; and

(iv) the inclusion of stress field and its coupling to non-uniform temperature field on the surface and in the bulk film.

The model and its extensions may prove useful in the theory and practice of crystal growth (pulsed laser deposition and laser assisted chemical vapor deposition), laser etching, and pattern formation on surfaces (self and induced assembly of surface structures), which have important applications in the fabrication of micro- and nano-electronic devices.

#### ACKNOWLEDGMENT

The author gratefully acknowledges Professor Brian Spencer for reading the manuscript in preparation and for the discussion.

[1] M. Siegert and M. Plischke, Phys. Rev. Lett. **73**, 1517 (1994).  
 [2] Y. Saito and M. Uwaha, J. Phys. Soc. Jpn. **65**, 3576 (1996).  
 [3] T. V. Savina, A. A. Golovin, S. H. Davis, A. A. Nepomnyashchy, and P. W. Voorhees, Phys. Rev. E **67**, 021606 (2003).  
 [4] H. Gao and W. D. Nix, Annu. Rev. Mater. Sci. **29**, 173 (1999).  
 [5] B. J. Spencer, P. W. Voorhees, and S. H. Davis, Phys. Rev. Lett. **67**, 3696 (1991).  
 [6] V. A. Shchukin and D. Bimberg, Rev. Mod. Phys. **71**, 1125

(1999).  
 [7] J. Krug, Adv. Phys. **46**, 139 (1997).  
 [8] L. Bartels, F. Wang, D. Moller, E. Knoesel, and T. F. Heinz, Science **305**, 648 (2004).  
 [9] F. Fournier, W. Zheng, S. Carrez, H. Dubost, and B. Bourguignon, Surf. Sci. **528**, 177 (2003).  
 [10] H. J. Ernst, F. Charra, and L. Douillard, Science **279**, 679 (1998).

- [11] O. Pierre-Louis and M. I. Haftel, *Phys. Rev. Lett.* **87**, 048701 (2001).
- [12] “Low-energy” in this context means that the incident energy is insufficient to cause (i) removal of adatoms from the surface, (ii) creation of surface defects, and (iii) melting of the surface.
- [13] W. W. Mullins, *J. Appl. Phys.* **30**, 77 (1959).
- [14] W. W. Mullins, *J. Appl. Phys.* **28**, 333 (1957).
- [15] J. W. Cahn and J. E. Taylor, *Acta Metall. Mater.* **42**, 1045 (1994).
- [16] M. M. Yakunin, *High Temp.* **26**, 585 (1988).
- [17] B. S. Yilbas and M. Kalyon, *J. Phys. D* **34**, 222 (2001).
- [18] S. R. J. Brueck and D. J. Erlich, *Phys. Rev. Lett.* **48**, 1678 (1982).
- [19] Z. Guosheng, P. M. Fauchet, and A. E. Siegman, *Phys. Rev. B* **26**, 5366 (1982).
- [20] N. C. Kerr, B. A. Omar, S. E. Clark, and D. C. Emmony, *J. Phys. D* **23**, 884 (1990).
- [21] N. C. Kerr, S. E. Clark, and D. C. Emmony, *Appl. Opt.* **28**, 3718 (1989).
- [22] V. I. Emel'yanov, *Quantum Electron.* **29**, 561 (1999).
- [23] Figures and data of Ref. [17] (where the material surface is not identified explicitly, but most likely it is metallic) show that the quasistationary state is achieved after just 3 to 4 laser pulses. Assume, for safety, that 400 laser pulses deliver the quasistationary state to the semiconductor surface, and  $\omega = 10^4 \text{ s}^{-1}$  [16]. Then, the characteristic time for the development of the quasistationary regime is  $\sim 4 \times 10^{-2}$ . This is four orders of magnitude less than the characteristic time of ripple relaxation,  $t_s$  (see Sec. II B).
- [24] M. Kasu and N. Kobayashi, *Appl. Phys. Lett.* **67**, 2842 (1995).
- [25] E. Hairer and G. Wanner, *J. Comput. Appl. Math.* **111**, 93 (1999).
- [26] W. Zhang and J. Vinals, *J. Fluid Mech.* **341**, 225 (1997).
- [27] To microscopic steps on a crystal surface.
- [28] V. B. Shenoy, A. Ramasubramaniam, H. Ramanarayan, D. T. Tambe, W.-L. Chan, and E. Chason, *Phys. Rev. Lett.* **92**, 256101 (2004).